Master's thesis

NTNU
Norwegian University of Science and Technology
Faculty of Information Technology and Electrical Engineering
Department of Electronic Systems

Eskild Jonatan Krumsvik Aanensen

Implantable e-compass for fish tracking field research

Master's thesis in Electronic Systems Design
Supervisor: Per Gunnar Kjeldsberg
Co-supervisor: Erik Høy
June 2023

Thelma Biotel AS

NTNU
Norwegian University of Science and Technology

THELMABIOTEL

Eskild Jonatan Krumsvik Aanensen

Implantable e-compass for fish tracking field research

Master's thesis in Electronic Systems Design
Supervisor: Per Gunnar Kjeldsberg
Co-supervisor: Erik Høy
June 2023

Norwegian University of Science and Technology
Faculty of Information Technology and Electrical Engineering
Department of Electronic Systems

NTNU
Norwegian University of
Science and Technology

NTNU
Kunnskap for en bedre verden

Department of Electronic Systems

TFE4930 - Master Thesis

Implantable e-compass for fish tracking field research

Author:
Eskild Jonatan Krumsvik Aanensen
Supervisor:
Per Gunnar Kjeldsberg
Co-supervisor:
Erik Høy (Thelma Biotel AS)

THELMABIOTEL

June, 2023

Preface

In this report the goal was to implement an accurate e-Compass for an acoustic fish tag. This was done as part of the course "TFE4930 - Electronic Systems Design, Master's Thesis" at the Norwegian University of Science and Technology in collaboration with Thelma Biotel AS. The task was given from Thelma Biotel AS, as a continuation of their work with acoustic fish tags.

This thesis is a continuation on the work in "Compass Heading for Implantable Fish Tag" [1]. That was where the deliberation on what sensor should be used, together with hard-iron calibration, noise measurements, choice of tilt-compensation algorithm, and estimated effect of latitude on heading accuracy.

Acknowledgements

This report relied on the help several people I would like to thank for the support.

Firstly my supervisor Per Gunnar Kjeldsberg for proofreading and helping direct the report.

Erik Høy and Eivind Brandsæter Hvam from Thelma Biotel AS for giving the assignment, and providing technical support and lending equipment.

Finally Oscar Nordahl a researcher at Linnéuniversitetet, for sharing the Pike fish acceleration dataset.

The report would be worse off without the help.

Abstract

Changes in an enviroment can have a huge effect on wildlife. Therefore monitoring it before and after a human alteration, can reduce the risk of negative effects caused in the area. Negative effects can be reduction in wildlife populations, destruction of nature, and reduction in food supply from fishing.

The compass direction will be useful in research on the effect of changes in an enviroment. Changes in pattern of the fish after engineering projects, such as dams, innfills, bridges, etc. It can also be used for studying fish in the natural enviroment, like how they navigate it or in the fish farming industry.

This thesis contains work towards the goal of implementing a tilt-compensated compass heading, on an ultra low-power fish tag. Using a 16-bit microcontoller with no floating point unit, and a combined MEMS accelerometer / magnetometer.

The main contributions are finding possible magnetic disturbances on the sensor, and possible solutions to those problems. Like the coil used in transmission, with its ferrite core it causes soft iron distortions, if placed near the sensor. This can be remedied by multiplying certain directions by a factor found during calibration. There is also the problem of during transmission of acoustic messages the coil will be magnetised in close proximity to the sensor, since the tag is exeptionally small, with only a few millimeters of space available. Meaning magnetic measurements should not be one during transmission to avoid invalid data; Luckily the field is not strong enough to cause permanent magnetisation to the components, which would have required the calibration to take place after a transmission. There is also the problem of the tag being started and stopped with a magnet, which can easily magnetise components making calibration necesary after use; This is impractical so other start/stop methods may need to be devised.

Furthermore solution to the problem of the tag not being inline with the direction of the fish, must be found; Due to it being loose in the stomach cavity of the fish. This report presents a solution using the forward acceleration of the fish, based on acceleration data from pikes, to correct small deviation to be more inline with the fish. A orientation precision of $\pm 4.5^\circ$ was found, but since there is no hard reference to compare aginst the accuracy can not be determined, only the relative precision.

Combining this with the magnetometer results found in the pre-project report of $\pm 3^\circ$ [1], the complete compass system should have a heading accuracy of ca. $\pm 7.5^\circ$, high enough to be useful in research.

Table of Contents

List of Figures

List of Tables

Chapter 1

Introduction

1.1 Motivation

Changes in an environment can have a huge effect on wildlife. Therefore monitoring it before and after a human alteration, can reduce the risk of negative effects caused in the area [4]. Negative effects can be reduction in wildlife populations, destruction of nature, and reduction in food supply from fishing.

The compass direction will be useful in research on the effect of changes in an environment. Changes in pattern of the fish after engineering projects, such as dams, infills, bridges, etc. [5]. It can also be used for studying fish in the natural environment, like how they navigate it or in the fish farming industry. Magnetic data could also improve geolocation of fish in the sea, by using known magnetism in the seabed [6], or improving dead reckoning by including direction.

In this paper *"Tag"* refers to the battery powered, logger, underwater acoustic transmitter, and telemetry device, developed by Thelma Biotel as a way to get information about fish in real-time. They are also used to monitor underwater equipment like: fishing gear, anchors, mooring lines, etc.

Such a system needs to be small, to even fit in most smaller fish. It also needs to be energy efficient, due to having no access to stable power from the electrical grid, or even less reliable sources like solar cell or similar. All that is available is a tiny battery. There is also a desire to make it timely, so useful information is available in real-time.

1.2 System description

As shown in Figure 1.1 the system is made up of an acoustic fish tag mounted loosely in the body cavity of a fish, transmitting acoustic messages to receivers hundreds of meters away [7]. The important components for this work are shown in a cross section of the tag, namely from top to bottom: The coil used to power the acoustic transmitter; The sensor a combined accelerometer & magnetometer (LSM303AGR); The controller a microcontroller from Texas Instruments (MSP430FR2476); And the battery used to power the device for months.

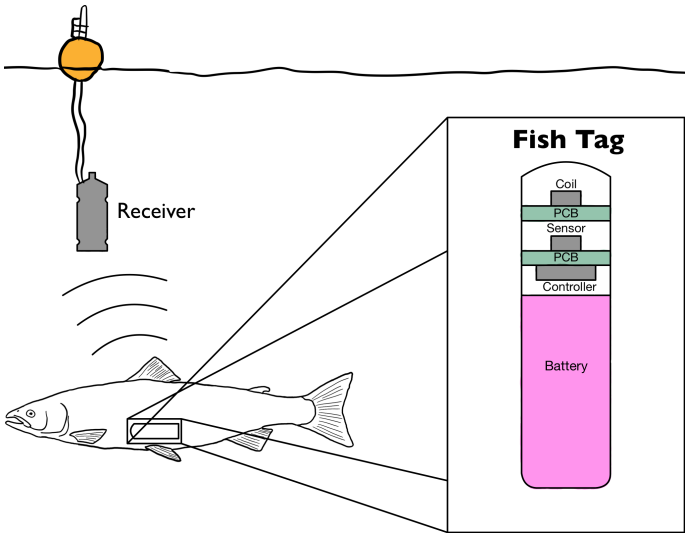

Figure 1.1: Simplified figure of system, showing fish tag internals, and location inside fish; Sending an acoustic message to receiver on buoy.

1.3 Objectives and limitations

The main objective of the work, was to find an energy effective way, of finding the compass heading of a fish. By expanding the functionality of the acoustic fish tags developed by Thelma Biotel AS. This includes:

- Using accelerometer data to find tag orientation relative to the fish frame of reference. This requires knowledge of the swimming patterns of the tagged fish.
- Measure magnetic distortions caused by other components on the tag. With a focus on the ferrite-cored coil used during acoustic transmission.
- Implement the system on the MSP430FR2476 to estimate the final accuracy, power draw, & memory footprint of the solution.

Limitations:

- No field tests were conducted on real fish.
- No external reference frames were known to compare against (magnetic north, fish direction).
- Accuracy must be high enough to have useful data collected, if it should be implemented, within $\pm 15°$ is definitely usable, based on other tags used in research [8].

1.4 Research method

Firstly a literature study was conducted. Then the magnetic distortion of two types of coils was measured, including hard and soft iron distortion, and while transmitting. The magnetizing effect of the magnet used to start and stop logging was also tested. Finally the orientation was to be found, based on accelerometer swimming data. By comparing subtracting the g-vector manually, and using a high-pass filter to filter it out. The direction was to be found by summing several values after a peak in activity. This was done since it could easily be implemented power efficiently in hardware. It was first tested on high acceleration attacks then later smaller peaks in continuos swimming.

1.5 Main Contributions

This work allows the acquisition of the compass heading by: finding and removing interference from other parts of the fish tag; Such as transmission, magnets, orientation, etc. The main contributions are finding possible magnetic disturbances on the sensor, and possible solutions to those problems. Like the coil used in transmission, with its ferrite core it causes soft iron distortions, if placed near the sensor. This can be remedied by multiplying certain directions by a factor found during calibration. There is also the problem of during transmission of acoustic messages the coil will be magnetised in close proximity to the sensor, since the tag is exceptionally small, with only a few millimetres of space available. Meaning magnetic measurements should not be one during transmission to avoid invalid data; Luckily the field is not strong enough to cause permanent magnetisation to the components, which would have required the calibration to take place after a transmission. There is also the problem of the tag being started and stopped with a magnet, which can easily magnetise components making calibration necessary after use; This is impractical so other start/stop methods may need to be devised.

Furthermore solution to the problem of the tag not being inline with the direction of the fish, must be found; Due to it being loose in the stomach cavity of the fish. This report presents a solution using the forward acceleration of the fish, based on acceleration data from pikes, to correct small deviation to be more inline with the fish. A orientation precision of $\pm 4.5^\circ$ was found, but since there is no hard reference to compare against the accuracy can not be determined, only the relative precision.

1.6 Report Structure

The report is divided in five parts:

2 Theory & Background, where background theory is introduced;

3 Previous work, how the system & its components currently work, and is used is presented;

4 Magnetism, method, results, and discussion related to magnetic distortion;

5 Orientation, method, results, and discussion related to orienting based on acceleration;

6 Finally the Conclusion of the report.

Chapter 2

Theory & Background

In this chapter there is some background information about:

- Magnetism and its effects, the difference between hard and soft iron distortion, types of magnetic materials like ferrite, how they become magnetised, and magnetic shielding. This is needed to understand potential disturbances to a compass.
- Microelectromechanical sensors, specifically an Anisotropic Magneto-Resistive (AMR) magnetometer, and an accelerometer, since these are used and discussed in the later chapters.
- Fish swimming modes, this is included to give explanation to what kinds of fish the system can be used in.
- Finally a Pike acceleration dataset from Linné University in Sweden, that will be used as a proxy for atypical fish.

2.1 Magnetic effects

This section describes magnetic properties and effects that are important to consider, due to the geomagnetic field being weak, leading the magnetometer to easily be affected by magnetic disturbances. The geomagnetic field is the magnetic field emitting from the Earth's core. It varies in strength, but stays close to half a Gauss, and points toward the magnetic north pole [9].

2.1.1 Magnetic distortion

Magnetic materials interference with the geomagnetic field by bending and shifting it, this is called magnetic distortion. It is further divided into two categories; hard iron, and soft iron distortion.

Hard iron distortion is caused by magnetic dipoles, shifting the local magnetic field off center. These magnetic fields can be caused by DC currents, permanent magnets, and batteries [10], as shown in Figure 2.1, a two dimensional plot the blue circle is moved from the origin.

Soft iron distortion on the other hand is caused by magnetic materials like iron and nickel, that bend the local magnetic field to go through them. This causes the magnetic field to be uneven, i.e. stronger in some directions [10]. Figure 2.2 shows the amplifying effect of soft iron on a magnetic field compared to an inert material like glass. This effect can cause the geomagnetic field being stronger in one direction with a soft magnetic material over a direction without, as shown in Figure 2.1 as a red ellipse.

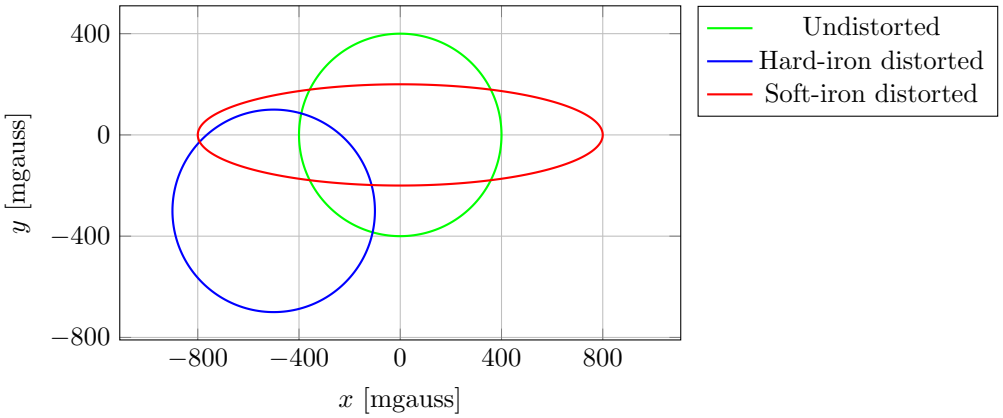

Figure 2.1: 2D example of magnetic distortions, the circles represent the readings from a magnetometer in the geomagnetic field with a strength of 0.4Gauss

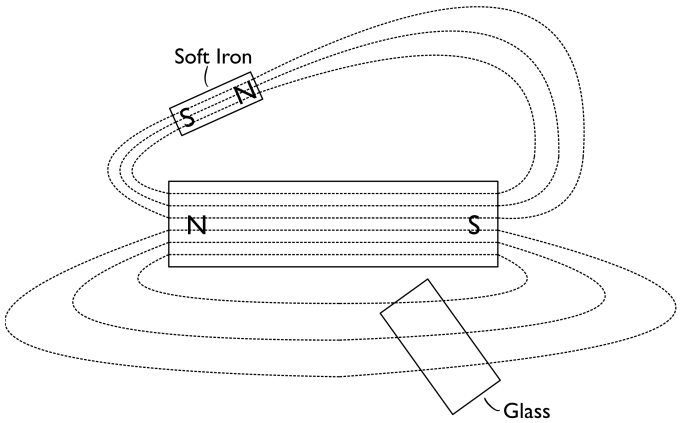

Figure 2.2: Magnetic field lines conducted through a soft magnetic material (iron), compared to a magnetically inert material (glass). Figure adapted from [11].

2.1.2 Hysteresis

Hysteresis is a term used for a material whose state is dependent on its previous state, its history.

Some materials like metallic iron are ferromagnetic, which means a material where all atoms align their magnetic moment when applied a strong magnetic field. There also exists ferrimagnetic materials like ferrite a ceramic mixture of iron oxide and other additives. These materials can usually not be as strongly magnetised as ferromagnetic materials, since the atoms align their magnetic moment opposing each other; They can only be magnetised if made up of two materials whose magnetic moment are unequal, causing a stronger field in one direction [13]. All magnetic material types is shown in Figure 2.4.

Remanence B_r: This is the magnetisation remaining after a large magnetic field is applied then removed [14]. read in Figure 2.3 at H(0). This value is high in strong permanent magnets, and low in transformer cores.

Coercivity H_c: This is how strong a field is needed to change the remanence to zero. Higher values means it is harder to reverse the magnetisation of the material. Unlike remanence however is the large span of values [14].

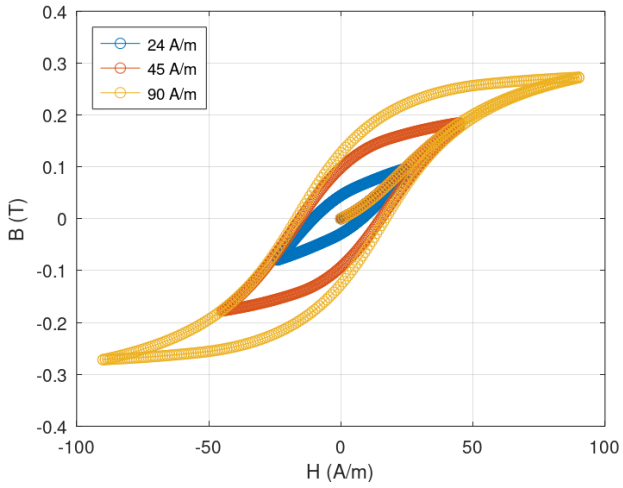

Figure 2.3: Simulation of ferrite being exposed to different strength magnetic fields. B Induction $[mT = 10 \cdot Gauss]$ against H magnetic field strength [A/m]. Figure made with octave script of Jiles-Atherton model of hysteresis [12]

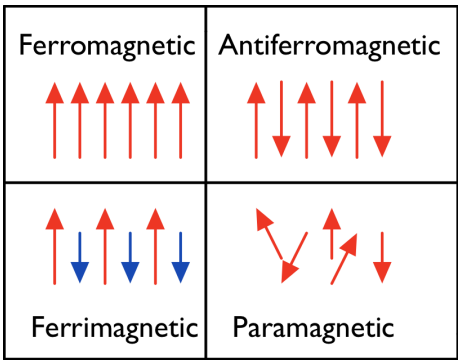

Figure 2.4: Types of magnetic materials

Inductor is a term used for a component with high inductance (hinders fast transition in currents), usually a coil of wire made of a conductive material.

Frequency in this context refers to how fast the inductor is switched on and off.

Soft magnetic materials is a term used for materials with low coercivity, meaning they can easily be magnetized and demagnetized. This allows them to be used at high frequencies, and low power. Another important characteristic of magnetically soft materials is the *power loss*, proportional to the area of the hysteresis loop. Low loss is the main indicator of a great soft material [14].

Hard magnetic materials is the reverse of soft materials, by being more stable in its magnetisation it can be used in permanent magnets [14].

2.1.3 Ferrite's magnetic properties

Ferrite is a ceramic material made with ferrous oxides Fe_2O_3 (rust) combined with metallic ions, to create a material with ferrimagnetic properties. Ferrimagnetic is different from ferromagnetic by having opposing magnetic moments, similarly to antiferromagnetic. Ferrimagnetic is different

from antiferromagnetic by having unequal strength of moments, causing some total magnetization to occur. This takes place when a crystal structure takes place with different forms of iron oxides $Fe^2 + Fe^3+$ [13].

Since ferrite is not a metal, but a ceramic, its resistance is substantially higher than its metal counterparts; Making it the ideal choice for higher frequencies, where eddy currents otherwise would be to high [15].

Hard ferrites like barium ferrite are used as permanent magnets, since their high coercivity allows them to withstand changes to their magnetization.

Soft Ferrites

Soft ferrites have low coercivity ($H_c < 100A/m$), meaning it can easily be coerced into aligning with an applied magnetic field. This property along with its high resistance ($1 - 10k\Omega m$), makes it the ideal material to be used at high frequencies. This includes any frequency above 100kHz up to the GHz range [15].

Some of ferrites downsides, that makes it unsuitable in lower frequencies, is its low maximum flux density ($B_s < 0.5T$). This property means it cannot contain strong magnetic fields without being saturated. Making it not the first choice in high power applications at lower frequencies, being outcompeted by pure iron [15].

The typical metals added to create soft ferrites are Zinc and either Manganese or Nickel [16].

Manganeese Zinc Ferrite Manganese Zinc Ferrite is used at frequencies below 5MHz. Instead of NiZn-ferrite for its higher flux density $B_s = 0.4T$, lower coercivity $H_c = 8A/m$, and higher permeability $\mu_{max} = 4000$. The resistance of $\rho = 1\Omega m$ makes it unsuitable for higher frequencies though, since the eddy loss is too great [17].

Nickel Zinc Ferrite Nickel Zinc Ferrite on the other hand because of its high resistance of $\rho = 10k\Omega m$ makes it suitable in applications above 2MHz up to GHz range. Its other properties makes it compare unfavourably, however ($\mu_{max} = 400, B_{max} = 0.25, H_c = 80A/m$) [17] except for its remanence ($B_r = 0.1T$) which can be a useful property.

2.1.4 Magnetic shielding

Shielding is done to reduce electromagnetic interference (EMI) for other components. by having most of the magnetic field go through a magnetically conductive material. Limiting the spread of the magnetic field H and the electric field E. This reduces the maximum flux B_s through the air. This reduces the maximum current that can be sent through the inductor, not ideal for power applications. Meaning a larger inductor must be used for similar results [2].

Electromagnetic radiation of an inductor in low frequencies below 30MHz is dependent on whether or not it is shielded [2].

The magnetic field H declines rapidly with distance, going down by the inverse cube $(1/r)^3$ where r is the distance. The electric field on the other hand, declines at a rate of the inverse square $(1/r)^2$ much slower in comparison [2].

Shielding requires space which will make an otherwise identical unshielded inductor smaller. Shielding also requires materials which could increase the price. A shielded inductor compared to an unshielded inductor with the same inductance have lower DC-resistance and saturation [2].

Shielded, semi-shielded, and unshielded There also exists semi-shielded which is a compromise between the two.

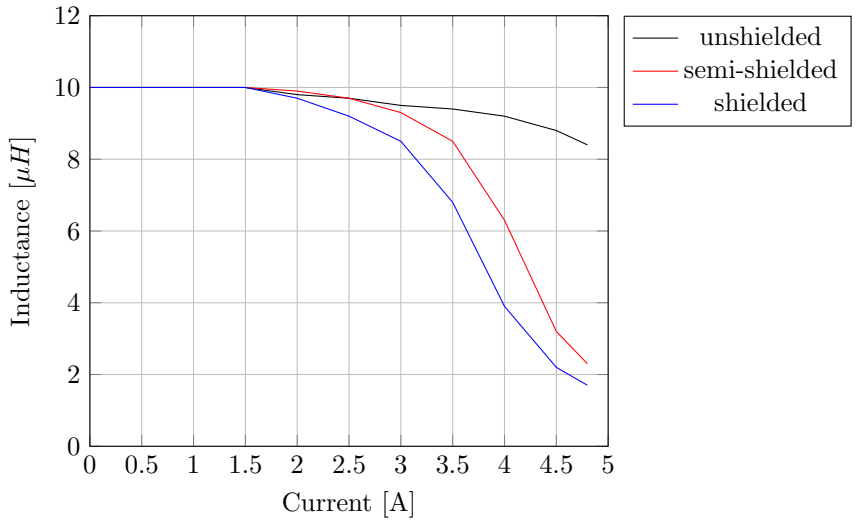

Figure 2.5: Saturation characteristics of different shielding in inductors [2]

Ferrites have low electromagnetic radiation at higher frequencies (above 1MHz), compared to metal inductors, especially NiZn [2].

2.2 MicroElectroMechanical Systems

The progress made in silicon manufacturing for the microchips, also made it possible to machine mechanical devices at micrometer scale [18]. This allowed creating sensors and actuators right on the silicon chip together with electronics hence Micro-Electro-Mechanical-Systems (MEMS).

MEMS have the potential of low-cost high volume production thanks to its batch processing manufacturing. It can also be made very high g shock tolerant, without post-shock performance degradation [19]. Mid to high performance open-loop MEMS accelerometer are today commercially available and reach tactical grade performances.

In this section the workings of the MEMS sensors used will be described.

2.2.1 Accelerometer

An accelerometer is a device that measures acceleration, this includes the static gravity of the Earth and the dynamic acceleration caused by speeding up and slowing down. Gravitation is an acceleration like any other with an average value of $9.81 m/s^2$ pointing straight down towards the Earth. The first MEMS accelerometer was designed at Stanford in 1979. They became more prevalent in the 1990s, outcompeting the previous piezo-electric sensors, because of their smaller size, lower power consumption, and robustness [20].

A linear accelerometer measures acceleration in one direction forwards and backwards. a tri-axial accelerometer measures in three different axis: X forwards backwards, Y side to side, Z upwards downwards. It is also possible to measure rotational acceleration, but then it is referred to as a gyroscope, and will not be covered in this report.

A typical MEMS accelerometer works by having a mass on springs and measuring the displacement with changes in the measured capacitance of mounted plates on the mass and fixed ones on the object [20]. This is shown in Figure 2.6, where the white background is a backplane to mount components, the beige object is the mass on springs with capacitive plates, and the coloured plates are there to measure the capacitance in each direction. When the large mass at the top moves by buckling the spring, the capacitive plates move closer to one set of measuring plates and further

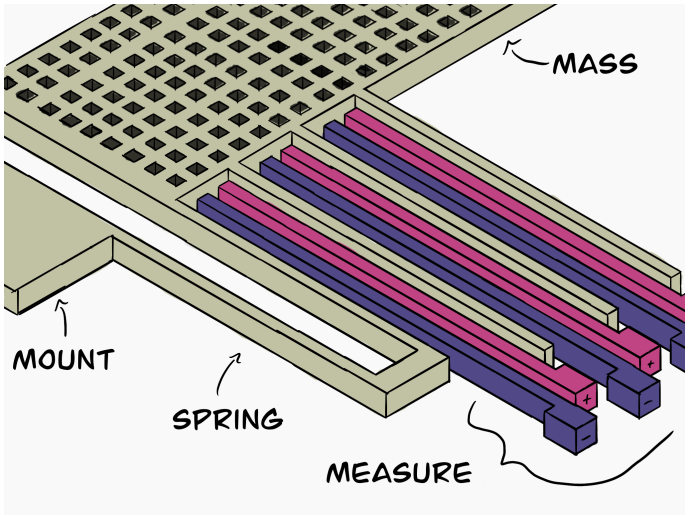

Figure 2.6: Typical MEMS accelerometer

away from others. This causes the capacitance to change measurably so the acceleration can be found [20].

In the gravity example, the mass will bend the spring a certain amount. If this coincides with the axis of the spring, it will be the full gravity vector and amount to ca. $9.81 m/s^2$.

2.2.2 Magnetometer

Many different types of magnetometers have been developed in recent years, including Hall-effect sensors, magneto-resistive (MR) sensors, and Lorentz force magnetometers. Lorentz force magnetometers can be fabricated in a standard silicon microelectromechanical systems (MEMS) fabrication process without any post processing or magnetic materials. As a result, they offer benefits over MR and Hall-effect sensors as they do not require magnetic materials and have no magnetic hysteresis. High sensitivity, low cost, low power, and direct integration with MEMS accelerometers and gyroscopes make the Lorentz force magnetometer, a very attractive option in consumer electronic devices that already contain these MEMS inertial sensors [21].

Anisotropic Magneto-Resistive (AMR)

The LSM303AGR uses an Anisotropic Magneto-Resistive or AMR magnetometer [22]. Uses the concept that a current has a different resistance depending on the direction and strength of a magnetic field going through the material [23].

2.3 Fish Swimming Modes

Fish are typically categorised into two swimming modes, either Median and/or Paired Fin swimmers, or body and/or Caudal Fin swimmers [24]. These two types are further distinguished in the next subsections.

2.3.1 Median/Paired Fin swimming

Median or Paired fin swimming is a type of swimming that mainly uses either: Median fins meaning single fins along the center of the fish, or Paired fins meaning mirrored fins on either side. Shown

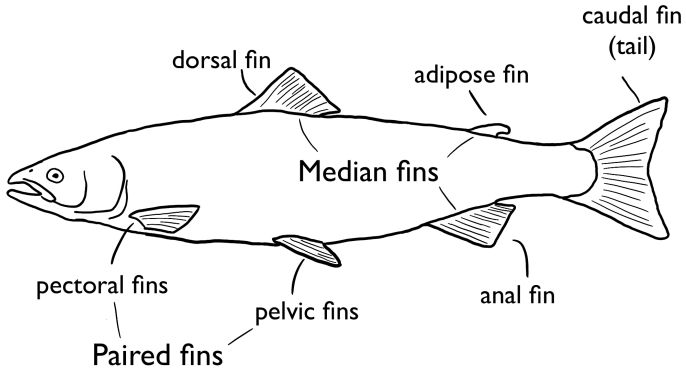

Figure 2.7: Fin terminology (Atlantic Salmon)

in Figure 2.7 are the most common types of fish fins. The median fins include the dorsal fin, adipose fin, and anal fin, while the paired fins are the pectoral fins, and pelvic fins Propulsion is achieved by either undulating the fins or flapping them. This type of swimming is preferred for slow manoeuvring, because of its increased agility, and efficiency.

2.3.2 Body/Caudal-Fin swimming

Caudal fin is the fin on the tail of the fish, also shown in Figure 2.7. It is mainly used in all fish for fast distance covering in straight lines, and fast acceleration for escaping predators or catching prey, but some fish also use it as their main propulsion. These fish are known as body or caudal fin swimmers. Below is a list of different types of caudal swimmers, and their descriptions. From Undulating to oscillatory:

Angilliform Whole body is used in a sinusoidal wave pattern, with at least one whole wavelength. named after eels Eel-like swimming [25] Example: Eels, Mud sharks

Subcarengiform Is like Angilliform where the whole body is used, but is not as flexible leading to only half a wavelength shows through. Example: Salmon, Cod

Carengiform meaning Kingfish-like, only rear half used in swimming. posterior [25] Example: Mackerel, Sardines

Thunniform meaning tuna-like, is a form of swimming where mostly the tail is used. peduncle and fin [25] Example: Tuna, Makosharks

Ostraciiform meaning boxfish-like is the most rigid form, only the tail is used for propulsion. The body cannot flex, going only in a straight line [25]. Example: boxfish, electric ray

Periodic/sustained swimming is used to cover distance. Transient swimming is used over a short time to escape predators or catch prey. Most fish use their whole body transiently, the examples use them sustained, as their main form of movement.

2.4 Pike Dataset

The acceleration data was gathered from the biology and environment institute of Linné university [26]. It contains five multiple gigabyte files of tri-axial accelerometer data from pikes. The dataset

has a resolution of 25Hz-50Hz, meaning the highest frequency data found will be half that at 12.5Hz-25Hz. The dataset contains acceleration data from 5 pike fish. Pike is a transient body caudal fin specialist [27], being an ambush predator it lays still waiting for fish to swim in front and then attack speedily with high acceleration [28]. A snippet of the dataset in table form is shown in Appendix A.

Pike number	Sex	Size [cm]	Log ID	Time period	Couple	Sample Freq [Hz]
1	Female	58	1	2020/02/05-19	NA	50
2	Male	45	4	2020/02/19-03/02	1	50
3	Female	59	5	2020/02/19-03/02	1	50
4	Male	51	3	2020/03/05-19	2	25
5	Female	53	2	2020/03/05-19	2	25

Table 2.1: Metadata for dataset

Chapter 3

Previous Work

3.1 Fish tag system

Thelma Biotel sells underwater ultrasonic acoustic transmitters and receivers, that communicate with an Open Protocol system at a frequency of 63kHz-77kHz [7].

3.1.1 Receivers

There are three types of receivers TBR 800, TBR 800 Release, and Live [29]. The receivers are all hydrophones, which mostly sit near the surface and store the data for periodic offloading or communicate with a computer via a wire.

3.1.2 Transmitters

There are plenty of options for transmitters, but they all are the same idea; They are fish tags consisting of a watertight housing with a battery, acoustic transmitter, a microcontroller, and various sensors. The transmitters are grouped into five categories based on their diameter: 6, 7, 9, 13, & 16 with the diameters: 6.3mm, 7.3mm, 9mm, 12.7mm, & 16mm respectively. These can all be further customized with different sensors, battery sizes, and transmitting strengths, changing the length of the tag [7].

3.1.3 System

The tags and receivers are already being used for different purposes today; Mainly they are used for tracking wild fish movement and behaviour, for research, but also aquiculture research, and management, like monitoring the welfare of the fish. They are also used in purposes beside tracking fish, some other uses includes: tracking fishing gear and nets, oceanographic instrumentation, water depth measurement, and infrastructure tracking of mooring lines & anchoring, cage weights in aquaculture, and net pens [7].

The goal of this thesis is to expand the functionality of the transmitter tags, with compass heading information. This has been a requested feature of their customers, for better research possibilities.

3.1.4 Fish tag mounting

Thelma Biotel chose to mount the tag loose internally, since it affects the fish less by causing less drag, than externally which would have higher energy expenditure. This does require them to cut open the fish to place the tag inside. It is also done since an external tag annoys the fish causing it to try and remove it by scouring. This alters the behaviour of the fish making research less

valuable as it cannot be applied as easily to non-tagged fish [30]. This does mean the tag is not fixed in orientation relative to the fish, making the orientation and therefore the compass heading harder to find easily.

3.1.5 MSP430FR2476 microcontroller

The main part of the system is a MSP430, which are low power microcontrollers from Texas Instruments. Various kinds are used by Thelma Biotel in their tags. They are used for their low power draw capability, going all the way down to a micro watt in standby. The specific model used is the MSP430FR2476 on a LaunchPad™ Development Kit. It is a 16-bit microcontroller with no floating point unit, running on 3.3V [31].

The smallest tag's microcontroller only has 16kB of storage, most of which will be used by other software. Therefore 4kB is set as a limit, to be able to fit the compass heading program in the memory of the smallest tag.

To increase the lifetime of the tag, hardware peripherals should be used as much as possible. Since dedicated hardware is almost guaranteed to be faster, and more energy efficient, or it would not have been included in the first place, because of the cost associated with making it. There are more peripherals that are used in the system, like timers, serial controllers, etc. that will not be discussed in this report.

3.1.6 Inductor Coil Core

Thelma biotel uses several different coils from the CB Series of Ferrite Power Inductors (SMD) from Taiyo Yuden [32]. It is used in the acoustic transmission system, and is on about every minute.

3.2 Specialization project

A pre-project was done prior to the master thesis work, titled "Compass Heading for Implantable Fish Tag" [1]. Relevant findings from this project is reported in the following sections, including: deliberation on what sensor should be used, noise measurements, hard-iron calibration, and simulation of the effect on accuracy based on magnetic field inclination.

3.2.1 Sensor deliberation

For the sensor the ST microelectronics LSM303AGR eCompass module was chosen. It is a combined tri-axial accelerometer & magnetometer. Combining the accelerometer and magnetometer allows for a reduction in size, cost and power draw, this is because the shared package saves costs on packaging, and allows for reducing pins by sharing buses, like: the power buses (Vdd, Vdd_IO, GND, C1), and the data buses for I^2C/SPI (SDA/SDI/SDO, SCL/SPC). Some pins need to be separate though like Chip select for SPI (CS_XL, CS_MAG), and interrupt pins (INT_1_XL, INT_2_XL) [3]. The static current in sleep is also considerably better than other options at only $2\mu A$ [3]. Especially ones with gyroscopes that have sleep currents above $1mA$. The sensor also works in a wide voltage range from 1.7-3.6 Volts, including the microcontrollers 3.3 Volts, meaning no signals need to be converted taking up unnecessary space. Speed is also no problem with a baudrate up to 3.4MHz, meaning the microcontroller is the limiting factor at 400kHz. The size is also exceptionally small at only 2x2x1mm, taking up a volume of only $4mm^3$ [1].

3.2.2 Noise measurement

A testbench was set up to measure the noise of the sensor, and the offset from origin. The test was conducted away from magnetic sources and ferromagnetic metals like iron. Since they will show up on the sensor measurements.

Low-pass filter or offset cancelation	bandwidth BW [Hz]	high-resolution mode Noise RMS [mG]	low-power mode Noise RMS [mG]
✗	ODR/2	4.5	9
✓	ODR/4	3	6

Table 3.1: RMS noise of operating modes (mG) [3]

The noise claims of the sensor datasheet (Table 3.1), were tested for the highest noise mode: Low-power, and the lowest noise mode: High resolution low-pass filtered. Both were measured for a minute laying still, with the data rate set to 10Hz. The results were mostly inline with the datasheet, only slightly higher at 9.9mG in low power, and 3.5mG in high-resolution low-pass mode.

3.2.3 Hard iron calibration

It is likely the sensor will be somewhat magnetised in production, offsetting the geomagnetic field. This is due to some hard iron magnetic distortion, described in Section 2.1.1. To compensate for this, simply subtracting a constant offset value from the X, Y, Z base values, found during calibration as shown in Eq. (3.1) [10]. This will center the uncalibrated values around the origin, causing more accurate measurements.

$$Corrected = Base - Offset \tag{3.1}$$

The offset value can be found by rotating the device in all directions, in an area with little magnetic interference, recording the maximum and minimum values for all three dimensions. The offset will then be the average of the two, as shown in Eq. (3.2). These values can then be set in hardware registers in the magnetometer, which will then perform the subtraction on all measured values [3] [1].

$$Offset = \frac{max + min}{2} \tag{3.2}$$

3.2.4 Simulated effect of geomagnetic field inclination

To determine the effect of an inclined geomagnetic field on the compass heading accuracy; A test was devised were typical values for the strength of the field for different inclinations were chosen, and the RMS noise of the sensor was included in a simulation, to determine the variability of the difference between a perfect sensor with no noise. This data was used to estimate the effect of inclination on heading accuracy. It was found the sensor is not very effective in arctic regions, if accuracy of single measurements is critical, but very effective everywhere else as shown in Table 3.2 [1].

field inclination	0°	73°	82°
heading error	±1°	±3°	±6°

Table 3.2: Geomagnetic field inclinations effect on compass heading error range [1]

Chapter 4

Magnetism

To find the compass heading of the fish, the geomagnetic field is used. It can be distorted by different effects however. This chapter tries to find and answer what magnetic disturbances are present in the tag, and the possible solutions for these problems.

Various tests were set up to find the extent of problems related to the magnetic field. This includes the Soft iron effects of the coils, at a couple of distances, and the effect of them powered during transmission. There is also a test related to the start and stop magnet's effect on various components of the tag, and if it causes significant magnetisation of the system that effect sensor measurements.

4.1 Large & small ferrite cored coil

A testbench was set up to measure the magnetic distortions, caused by two sizes of ferrite cored coils, which one of either is used during acoustic transmission. A sectional view of the coils is shown in Figure 4.1.

(a) without light (b) with light

Figure 4.1: Cross section of cut open copper coils, surrounded in ferrite.

The coils contain ferrite to boost their effective Henry level, this allows for a smaller coil to be used, compared to one with an air core, important in this application. The reason ferrite makes a good core material, is that it is a great conductor of magnetic fields. This reason is exactly why it causes problems with the sensors ability to measure the geomagnetic field. The ferrite conducts the field away in certain directions, and towards in others, making the field uneven in strength, depending on the direction. The coils have this effect when unpowered, but are an even bigger problem while powered, since they will generate a magnetic field. Both of these effect will be studied in this section, and to what extent they pose a problem.

To test them the coils were taped on top of the sensor one at a time, including no coil as a reference,

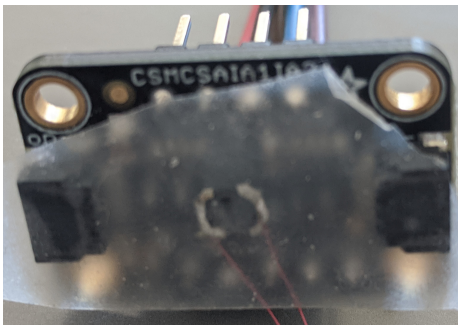

Figure 4.2: Large coil taped over sensor

to imitate the close proximity in the final product, shown in Figure 4.2. This will give the worst case scenario, since the magnetic effects are larger the closer they get.

4.1.1 Soft iron effect of coil

They were then spun in circles for one minute separately, and logged at a 100Hz polling by the sensor, to find the soft iron distortion of the coils. The magnetometer can measure up to 50 Gauss with a resolution of 1.5mGauss. The coils were not transmitting at the time and were not even connected to the rest of the tag at all, to exclude any chance of being powered. The results of this test is shown in Figure 4.3. The 'empty' graph is a control with no coil distortion creating a sphere. The large coil seems to not change z axis readings, but halves readings in the x, and y directions. The small coil is similar, but to a slightly lesser extent.

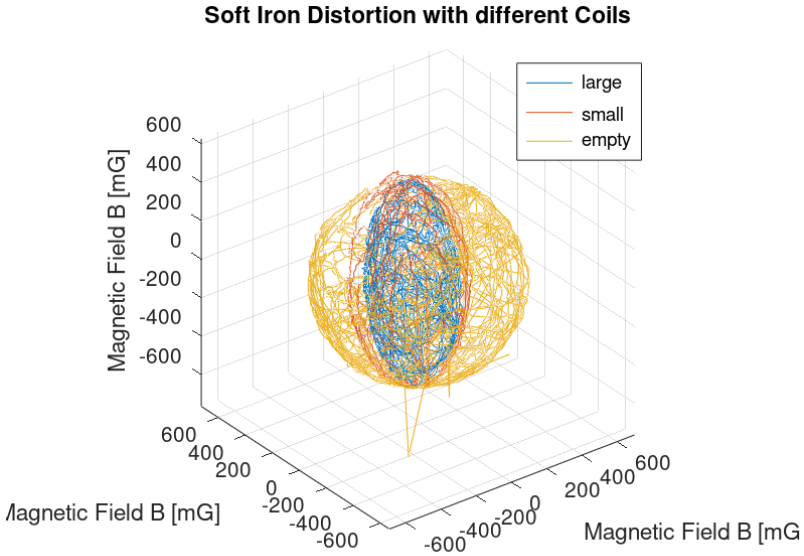

Figure 4.3: Magnetometer readings while rotating with different Coils directly above sensor.

4.1.2 Transmission

The distortion measured so far, happens even when the coils are unpowered, but when powered the coil emits a magnetic field, it will also distort the geomagnetic field. To test this, the coils where taped on in the same position, but this time the tag was connected to the two leads coming off the coil, to power it on intermittently, like in the final product. The tag was set to transmit 10 pulses every 10 seconds, and was measured by the sensor at 100Hz polling for one minute. The

results are shown in Figure 4.4, there it is shown that transmission did not magnetise the coil permanently, but is too strong to allow reading the magnetometer during transmission, since the pulses are more than twice the strength of the geomagnetic field at around 500mGauss.

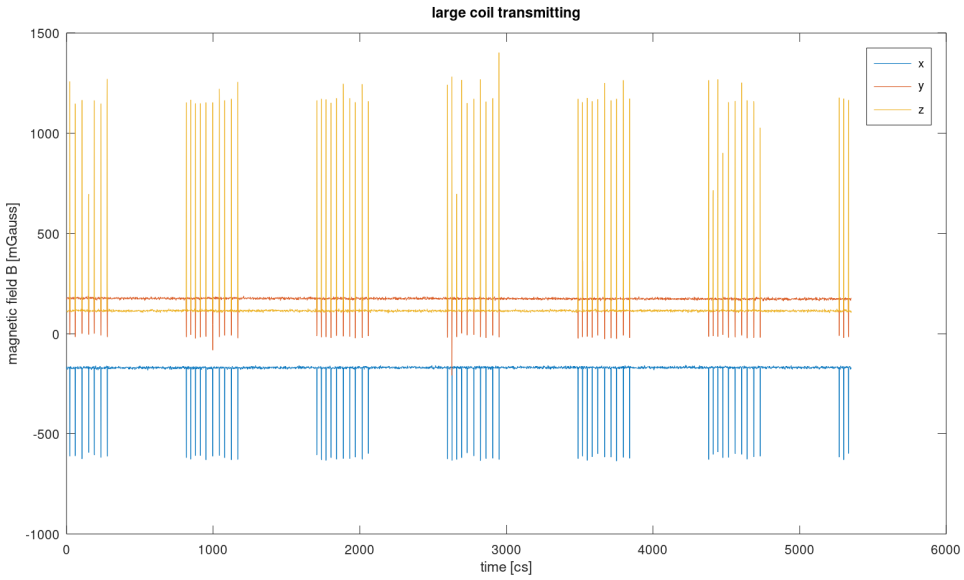

Figure 4.4: Test if acoustic transmission magnetises coil.

For the second test the tag was unplugged and plugged back in with differing polarity to test whether the coil was already magnetised in the previous direction. As shown in Figure 4.5, the magnetic field remains constant except for the pulses, and slight rotation caused by plugging in and out the coil.

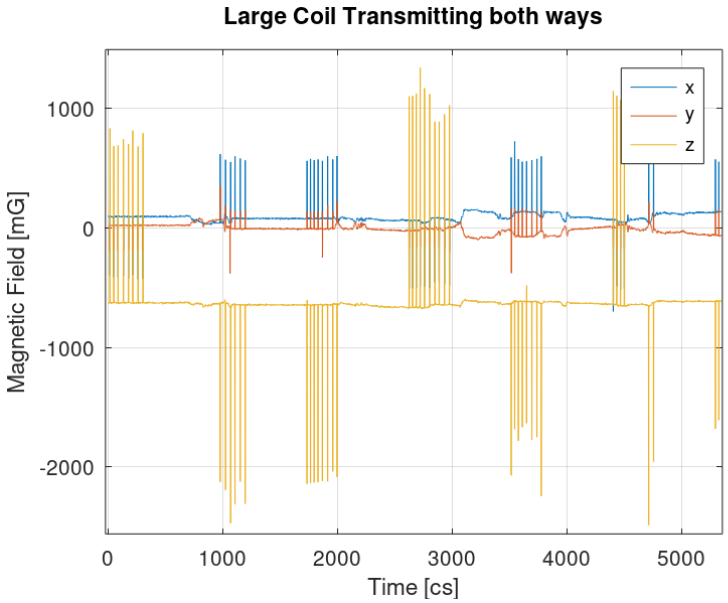

Figure 4.5: Test if acoustic transmission magnetises coil.

4.1.3 Placement

To check whether a small difference in placement would affect the magnetometer greatly due to the rapid drop off from the magnetic field relative to the distance. A test to measure the magnetic

field near the coil and slightly further away, to see the difference if mounted next to compared to the other side of a PCB. The large coil was then mounted on a 1mm thick plastic card to measure the difference from one side to the other. Testing the difference of no distance compared to a small gap, to test if the coil should be mounted farthest away possible from the sensor. The small size of the fish tag makes it unfeasible to mount very far away, where the effect is negligible, but small changes are possible.

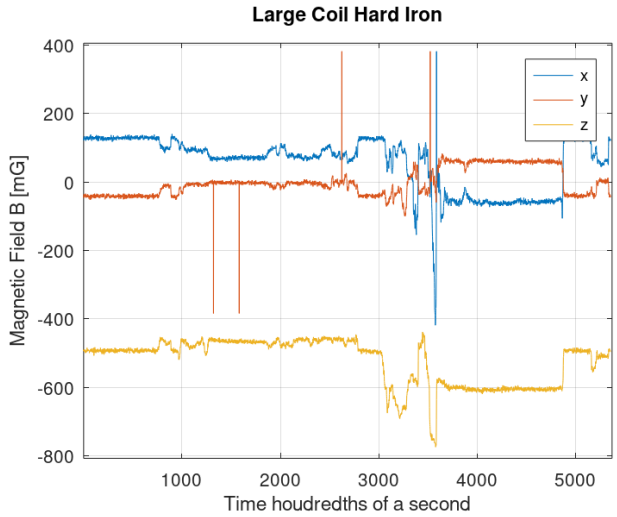

Figure 4.6: Difference in magnetic distortion based on distance (Large Coil)

Figure 4.6 shows first no coil in the first 8 seconds, then no gap 8-27 sec, and finally a 1mm gap from 36-49 sec before returning to no coil. The field actually became stronger at a greater distance, meaning the turning of the coil probably had a greater effect than expected. This might be due to the casing being, different or the coil being magnetised. The effect is very slight however and wont effect the accuracy enough to worry about.

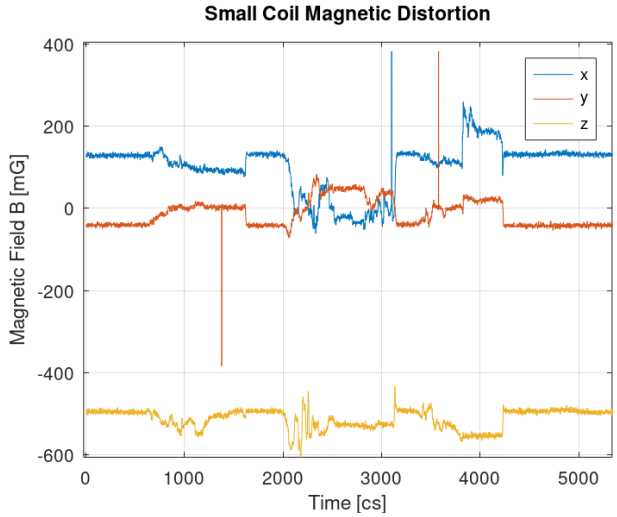

Figure 4.7: Difference in magnetic distortion based on distance (Small Coil)

Discussion

These results shows the need for a soft iron calibration where the x and y directions need to be boosted in software to compensate for weaker values, or the accuracy will suffer at least to an extent, in certain directions.

4.2 Start and stop magnet

Currently the fish tag is being started and stopped, by pointing a strong magnet near it. This may cause issue if said magnet magnetising parts of the tag permanently, effectively ruining any prior calibration done. Therefore several tests were done to quantify this problem. To test if the start and stop magnets could magnetise any components significantly, both the tag, and sensor were measured before, during, and after exposure to the magnet.

4.2.1 Tag magnetisation after normal use

For the first test the tag was placed on top of the magnetometer sensor and rotated in all directions near the top, center, and bottom, to find its magnetisation level after normal use shown in Figure 4.8.

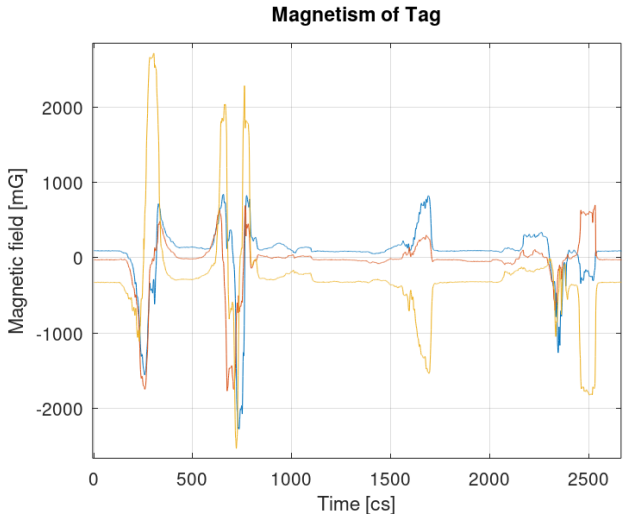

Figure 4.8: Tag magnetisation after normal use.

The test shows that the tag already was magnetised by the magnet after stopping and starting transmission earlier to see if the tag worked properly. The tag contains ferromagnetic material like steel in the battery casing which has been magnetised to several Gauss during normal use, several times greater than the Earth's magnetic field of just half a Gauss.

4.2.2 Applying the magnet to the tag

For the second test the tag was rotated along the center, then a magnet was applied shown in Figure 4.9 (at 16.7s - 17.3s) to test if it would be magnetised, then again rotated around the center (17.7s - 18.6s).

The magnetometer measured a magnetic field of -42 Gauss at the peak of applying the magnet even through the tag itself. The tag became magnetised with a value of several Gauss much greater than the first test. This would be because the magnet was applied much closer to get the maximum effect possible. Before the previous test the tag was started and stopped to test transmission, this included starting the tag with the magnet, but that time the magnet was only brought close enough to start the tag, applying a weaker field.

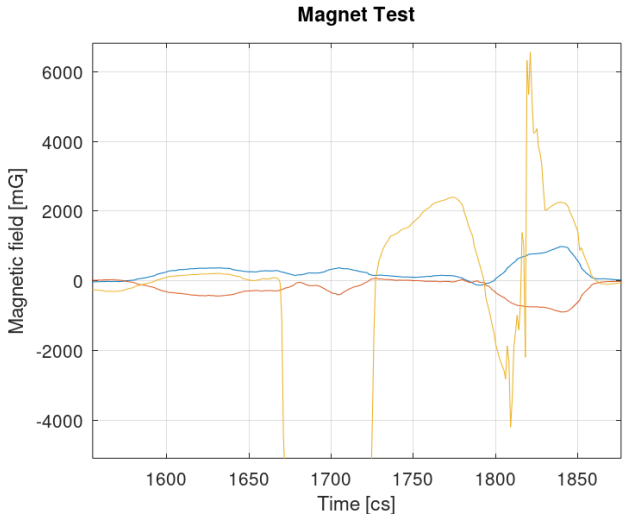

Figure 4.9: Used magnet to try and magnetise Tag.

4.2.3 Applying the magnet to the sensor board

In the third test the magnet was applied to the sensor breakout board directly to see if it would be affected. The chip itself could be affected being an AMR magnetometer, meaning it contains materials with magnetic properties. The metal soldering pads around could also potentially be magnetised.

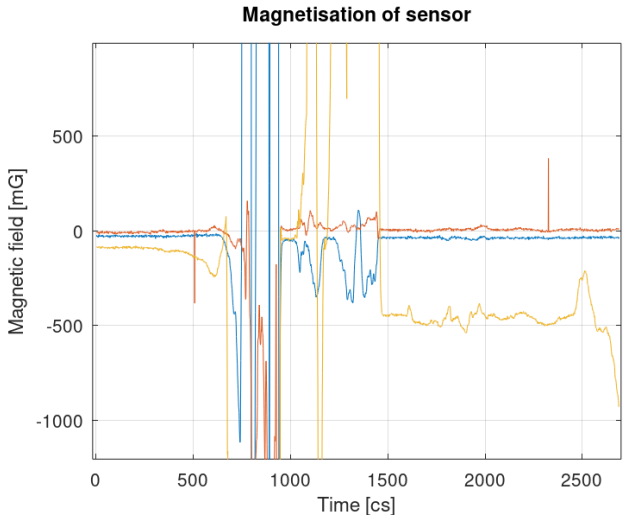

Figure 4.10: Test if sensor breakout board could be magnetised.

As shown in Figure 4.10 the sensor itself also gets magnetised by half a Gauss 500 mG enough to make sensor readings unusable, since it is the same strength of the geomagnetic field, making the compass not able to point in half of all possible directions.

Discussion

The magnet causes significant permanent magnetisation of the tag, a hard iron distortion that has to be remedied by calibration after being applied, since the tag is started by using a magnet this will require in field calibration, or a new way of starting/stopping the tag.

Chapter 5

Orientation

The goal of this chapter is to find the direction of the fish based on accelerometer measurements. The direction will then be used to correct the magnetometer reading to be aligned with the fish instead of the tag, since the tag may not be in direct alignment with the fish, and can move ±30° based on Thelma Biotel's experience. This will allow accurate heading even when the tag is not aligned with the fish.

5.1 Method

To chose the method to find direction based on acceleration, The method will have to vary depending on species since behaviour of fish are different, like swimming pattern, amount swam, etc. Forward acceleration was first assumed as constant, and therefore needed to be found from sway of the fish. This was based on the most common fish that are tracked by Thelma Biotel, atlantic salmon, and similar fish. The dataset acquired was for pikes however, pikes are ambush predators, and are body caudal fin transient specialists [27], laying still most of the time with some rare activity grabbing food, and looking at the data the previous assumption was not true, a new approach was needed.

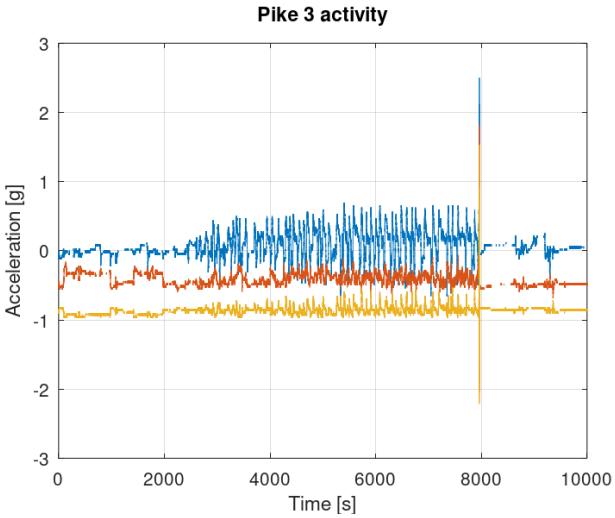

Figure 5.1: Two and a half hours of activity of Pike 3, before and after are large periods of no activity.

At first a solution of using the high acceleration spurts in attacks (1-3g), was viewed as shown in Figure 5.1 as a 2g spike at 8000s. It would be easy to filter in the high acceleration, with a threshold activity detection on the sensor, and the infrequency would ensure low energy expenditure. The compass heading would also be less likely to change, in the more relaxed periods between the spurts of activity. The solution has certain problems however, the chaotic movement might cause the tag

to moving during the event, making the measurement not accurate to the orientation of the tag after the event. This combined with the low frequency of measurements, could cause the tag to be less accurate for long periods of time, if accurate at all.

A new solution was proposed using the more slow and steady swimming (ca. 0.5g), shown in Figure 5.1 as a periodic signal from 3000-8000s. The higher frequency would cause higher energy expenditure, but this could be compensated for by requiring less measurements and processing than the previous solution, since the forward acceleration is clearer, and not obfuscated by side to side sway, and up and down heave, like the spurts.

5.2 Results

This section contain the results of trying to find direction. There is no way to verify accuracy, since there is no reference to go by except for the g-vector, which has no direction information. Meaning the results only show the relative precision of the methods.

5.2.1 Direction based on high acceleration attacks

At first an attempt to find the direction based on high acceleration attacks was made. The data has intermittent some spikes in acceleration above 1g up to 3g, these are easy to filter in, since they are larger than 1g meaning the gravity vector (g-vector) is not large enough to trigger a false positive. They also happen infrequently meaning power consumption should be the lowest possible. A downside with this implementation is the infrequency of attacks, causing large gaps between calibration of the tag orientation, leading to inaccurate results.

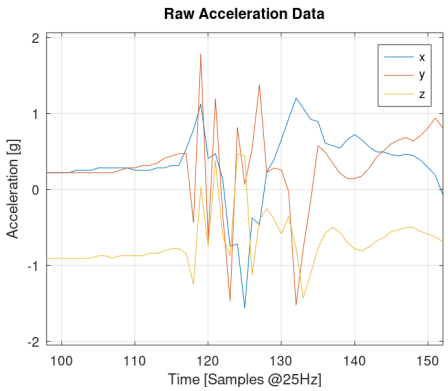

(a) Raw accelerometer data

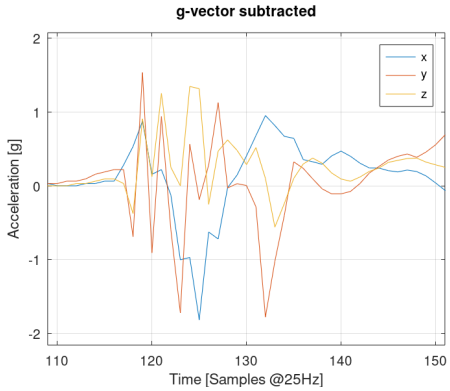

(b) Subtracted g-vector from all points

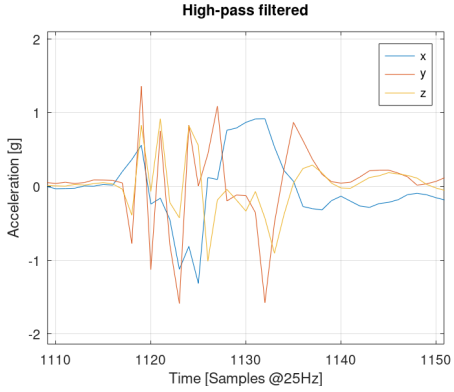

(c) High pass filter to remove sub 1Hz frequencies

Figure 5.2: Attack spurt data from pike 5

Looking at the pike 5 dataset in Table 2.1 an attack with similar g-vector before and after was chosen as shown in Figure 5.2a, since the tag seems like it stayed in the same orientation through the whole time. This makes it possible to use the acceleration from the very start, as representative of the g-vector in the data, and by subtracting it from all points, will separate the acceleration of the fish from the g-vector, meaning only the pike's movement is visible, as shown in Figure 5.2b.

High-pass filter

This would be hard to do in firmware on the tag however so an easier implementation that uses the hardware high-pass filter would be easier to achieve. To simulate this a similar filter to one possible on the sensor was created as shown in Figure 5.3. The result after filtering is shown in Figure 5.2c, it should not be to different from Figure 5.2b where the g-vector was subtracted manually, just the X axis acceleration peak who stayed in the same direction for a longer period, is somewhat reduced.

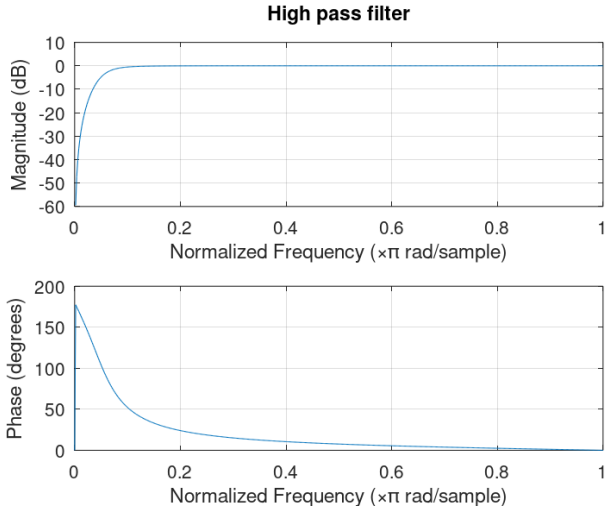

Figure 5.3: High pass filter frequency response

The Butterworth high-pass filter used was made using a script from Octave Forge [33], shown in Appendix Section B. The sample rate was set to 24Hz, instead of 25Hz since odd numbers does not work, since the first step is to divide by two and floats are not supported for all functions. The stop frequency was set to 0.1Hz and pass frequency to 1Hz. This gave a minimum of a 3rd order butterworth filter needed to work. This should be somewhat similar to the high-pass filter of the sensor, which has an adjustable cut-off frequency from 0.05Hz to 1 Hz at 25-50Hz as shown in Table [34].

Relative precision of direction vectors

A major concern of looking at the spurt acceleration is the large oscillation of the Y component, and to lesser extent X, and Z. This could easily cause the orientation to be misaligned to the left or right, the most important direction for heading. To mitigate this as many values as possible should be summed together to hopefully cancel out the unwanted noise. The FIFO-buffer of the accelerometer can store 32-values before overflowing, enough to store the important large acceleration shown in Figure 5.2 easily, especially at this low sampling rate dataset at 25Hz.

Figure 5.5 shows the different vectors found in three dimensions. The length and up and down differences are large, due to the reduced value of the high pass filtered version, but as shown in Figure 5.4 the difference in direction relative to the g-vector is minor. It is still large enough to cause issue however, since it combined with the magnetometer error adds up. Due to this and problems with infrequency, another method was chosen to be further studied.

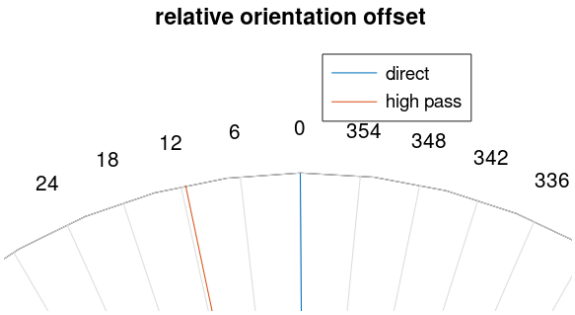

Figure 5.4: Difference between high pass filtered direction vs direct. Direct here referring to the subtracted gravity vector result.

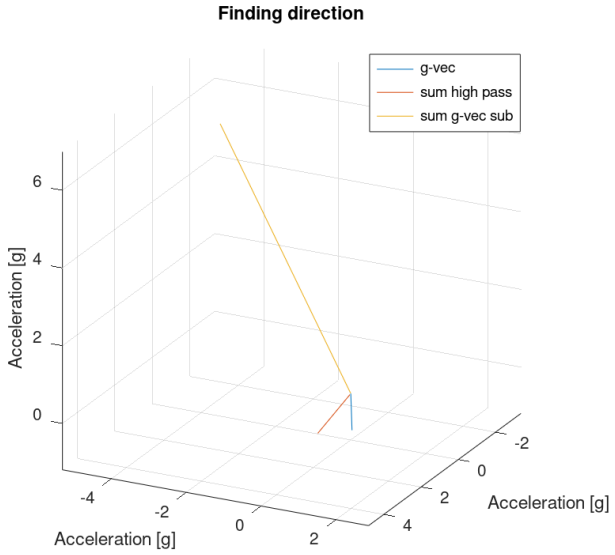

Figure 5.5: Direction found with high-pass filter and subtracting g-vector compared to g-vector.

5.2.2 Direction based on periodic slow swimming

For the second attempt a higher sampling rate dataset was chosen this time from pike 3 as shown in Table 2.1, the sampling rate is 50Hz. The time chosen is a period with calm regular swimming before an attack. As shown in Figure 5.6 the data is taken from a period of over half an hour of calmer low acceleration swimming with frequent peaks every minute and a half. This section was chosen since it is pretty uniform in timing of peaks, height, and the g-vector is pretty consistent from start to finish. The Y component shows no sign of rapid large oscillation as in the spurts, so summing is not a requirement leading to possible lower power consumption by taking fewer measurements with less processing.

To find the gravity vector here, a fourier transform was performed and the first component compared to a value taken before the swimming started. When they were shown to be similar, the three most significant numbers aligning, the average value of the dataset, or the first component of the fourier transform was used as the g-vector.

To find the direction all X values below 0.5g was filtered out leaving 15 peaks, these were then summed and rotated so the g-vector pointed straight down. The rotation was done using rotation matrices, first rotating g-vector around the Z axis to align with X axis then rotated around Y axis to point straight down. Decided also to use acceleration directly to measure difference from peak to peak, since high pass filtered version is more sensitive to speed of rise/fall. This created 15 different direction to be compared as shown in Figure 5.7 and Table 5.1.

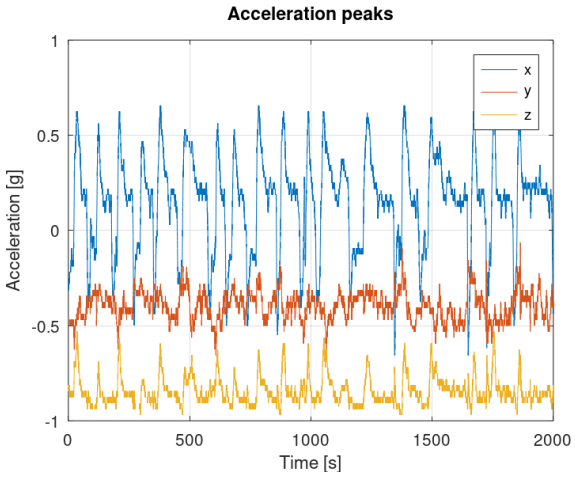

Figure 5.6: Dataset used for analysis, a peak comes around every 100 seconds. This is a subset of the data shown in Figure 5.1.

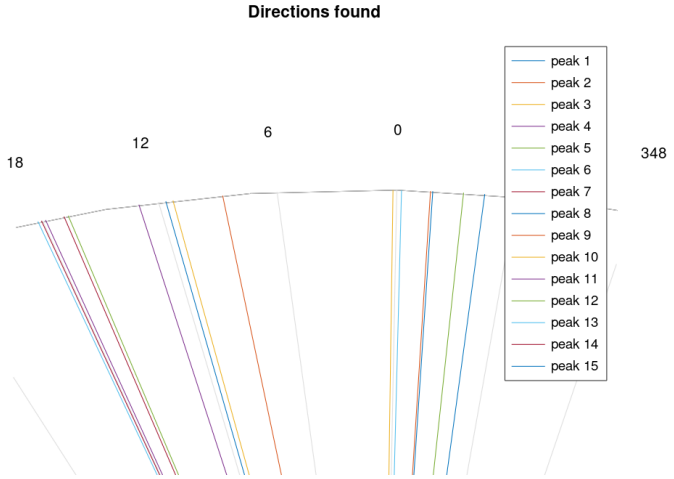

Figure 5.7: Difference between different peaks of acceleration.

Discussion

Consecutive peaks are not close together, so it seems the tag did not drift slowly over time. The peaks do seems to group however, potentially showing a few different orientations. The directions are mostly clumped around 12 and -2 degrees, making me think the tag was not stationary, but moving between to orientations. Assuming this the maximum spread is only 9 degrees or ± 4.5 degrees, plenty small enough to be useful even aggregating with the error of the magnetometer. However it is not possible to know if this assumption is true therefore assuming the worst case scenario of the tag being stationary, the maximum increases to 22 degrees or ± 11 degrees, that is too great for a useful compass. However the assumption of stability also means the large swaying from left to right are associated, meaning they can be averaged together to make better prediction.

$$FIRfilter = [\frac{1}{3}, \frac{1}{3}, \frac{1}{3}] \tag{5.1}$$

$$center = \frac{max + min}{2} = \frac{18.24 - 4.41}{2} = 6.91 \tag{5.2}$$

A simple low pass filter of averaging three values together adding the current and two previous measurements, the accuracy falls in line with the previous accuracy of ± 4.5 degrees, making it also

Peak Number	Relative Tag Orientation
6	18.2357°
14	18.0507°
4	17.8368°
7	16.8707°
12	16.6503°
11	13.0028°
1	11.6274°
3	11.2640°
9	8.7434°
10	0.1893°
13	−0.2374°
2	−1.6897°
8	−1.8032°
5	−3.3471°
15	−4.4114°

Table 5.1: Relative difference between the found orientation of different peaks.

a viable strategy. This averaging does have a downside in increased processing however, and in the event of a large fast shift in orientation some values will be wrong for a short time. The averaging was done as a FIR filter as shown in Equation 5.1. The true orientation is assumed to be in the center of extremes, and calculated in Equation 5.2. The final results is shown in Table 5.2.

Peak number	Relative tag orientation
14	4.5779°
8	4.1911°
6	3.9985°
7	3.6764°
12	3.0375°
13	2.8952°
4	2.2270°
5	1.6746°
1	1.5725°
3	0.1572°
9	1.0270°
11	0.4018°
2	−1.2941°
15	−2.4427°
10	−4.5335°

Table 5.2: Rolling average results (3 values) centred.

These direction values should be added on to the magnetometer readings as an offset, to further improve the accuracy of the compass heading, even if the tag is not aligned with the direction of the fish. They should not be centred however, that was only done to show the range of error, in the solution. Adding together the precision of the magnetometer ($\pm 3°$) and the orientation system ($\pm 4.5°$), gives a total precision of $\pm 7.5°$, half that of other fish tags. This does not include loss based on resolution however, which will add another degree ($\pm 1°$) assuming 8-bit encoding, since ($360 > 255$) meaning only even degrees can be included.

Another gripe with this solution, is the need for the g-vector to align the data. This requires that the g-vector needs to be found often in firmware, when as few measurements should be taken as possible. A possible solution to this, could be checking if the absolute acceleration vector length equals 1g, when measurements are taken at periodic intervals. This would work easily for the pike, seeing that it lays still most of the time leaving the g-vector often undisturbed. This could be trickier for other fish who stay moving all the time, causing a more chaotic signal, requiring more measurements or processing for low-pass filter or similar.

Chapter 6

Conclusion

The compass heading tag could be used in plenty unforeseen ways, but this thesis tailors the results for wildfish research. Researchers could use direction data for many purposes, and the acoustic transmission allows for real-time data retrival allowing for more possiblilities. Competing products have an accuracy of $\pm 15°$, and only log the results locally and need to be retrieved at a later date.

In this work acceleration and magnetism data were used in conjunction to find a compass heading. This will be used to further research on fish, or track underwater equipment. The acceleration data of pike fish, were used to find a way of estimating the relative orientation of the sensor tag, compared to the fish. This offset will then be added to the magnetometer reading, to align the heading with the fish instead of the tag. The calibrated magnetometer is then used to find the compass heading, pointing to magnetic north. This can later be adjusted to true (geographic) north, if the time and place is known.

Based on the findings in this report, it should be possible to use this system to get a precision of $\pm 7.5°$, by adding together the precision of the magnetometer ($\pm 3°$) and the orientation system ($\pm 4.5°$). The start and stop magnet should also be replaced to another solution, like a weaker magnet, using the accelerometer to find tapping, or another method, since the magnetisation of the strong magnet is hard to predict, and calibrate for in the field. The location and type of coil is unimportant, as long as it is powered off during measurement, and proper soft iron calibration is conducted.

This meets most of the goals of the thesis, but the firmware implementation and energy measurements where not completed. The stated precision also had no reference to compare to meaning no total accuracy can be found.

6.1 Further Work

To finish this work, the system should be implemented on a tag and tested on real fish. This includes implementing it completly in firmware; Measurering the active and inactive power consumption; Estimating energy expenditure and lifetime with different size batteries; And Finally testing the system on real fish, idealy with an external reference to compare results against.

Bibliography

[1] E. J. K. Aanensen, "Compass heading for implantable fish tag," Pre-project, NTNU, Dept. of Electon. Syst., Trondheim, Norway, 2022, unpublished.

[2] R. Bramanpalli, "The behavior of electro-magnetic radiation of power inductors in power managment," Würth Elektronik, Waldenburg, Germany, Tech. Rep. ANP047b, 2018. [Online]. Available: https://www.we-online.com/catalog/media/o109027v410%20ANP047b%20EN.pdf

[3] ST microelectronics, *Ultra-compact high-performance eCompass module: ultra-low-power 3D acceleromter and 3D magnetometer*, 11 2018, rev. 10.

[4] J. Radinger *et al.*, "Effective monitoring of freshwater fish," *Fish and Fisheries*, vol. 20, no. 4, pp. 729–747, 2019. [Online]. Available: https://onlinelibrary.wiley.com/doi/abs/10.1111/faf.12373

[5] J. G. Davidsen, M. Husby, and A. Foldvik, "Konsekvenser for sjøørret, villaks og fugl ved utfylling av deler av elveosen til stjørdalselva. kunnskapsoppsummering og foreløpige forslag til avbøtende og kompenserende tiltak," NTNU Vitenskapsmuseet, natur notat, 9 2020.

[6] J. Nielsen *et al.*, "Potential utility of geomagnetic data for geolocation of demersal fishes in the north pacific ocean," *Animal Biotelemetry*, vol. 8, pp. 1–20, 2020.

[7] Thelma Biotel AS. Transmitters. [Online]. Available: https://www.thelmabiotel.com/transmitter/

[8] Star Oddi. (2017) Compass, tilt (3d), temperature and depth archival tag. [Online]. Available: https://www.star-oddi.com/products/data-loggers/fish-geolocation-magnetic-tag

[9] C. C. Finlay *et al.*, "International Geomagnetic Reference Field: the eleventh generation," *Geophysical J. Int.*, vol. 183, no. 3, pp. 1216–1230, 12 2010. [Online]. Available: https://doi.org/10.1111/j.1365-246X.2010.04804.x

[10] V. Renaudin, M. H. Afzal, and G. Lachapelle, "Complete triaxis magnetometer calibration in the magnetic domain," *J. of Sensors*, vol. 2010, 2010.

[11] Museu das Comunicações. (2022) The magnet and the magnetic field. [Online]. Available: http://www.cmm.gov.mo/eng/exhibition/secondfloor/MoreInfo/2_2_1_MagneticFields.html

[12] D. C. Jiles and D. L. Atherton, "Theory of ferromagnetic hysteresis," *J. of Magnetism and Magn. Mater.*, vol. 61, no. 1-2, pp. 48–60, 1986.

[13] W. P. Wolf, "Ferrimagnetism," *Reports on Progress in Physics*, vol. 24, no. 1, pp. 212–303, jan 1961. [Online]. Available: https://dx.doi.org/10.1088/0034-4885/24/1/306

[14] G. Bertotti, "Chapter 1 - magnetic hysteresis," in *Hysteresis in Magnetism*, ser. Electromagnetism, G. Bertotti, Ed. San Diego: Academic Press, 1998, pp. 3–30. [Online]. Available: https://www.sciencedirect.com/science/article/pii/B9780120932702500507

[15] N. A. Spaldin, "Ferrimagnetism," in *Magnetic Materials: Fundamentals and Applications*, 2nd ed. Cambrige, UK: Cambridge Univeristy Press, 2011, pp. 113–132.

[16] Ferroxcube. (2008) Soft ferrites introduction. [Online]. Available: https://ferroxcube.home.pl/prod/assets/sfintro.pdf

[17] H. Skarrie, "Design of powder core inductors," Licentiate Thesis, Lund Univ., Dept. of Ind. Elect. Eng. and Automat., Lund, Sweden, 2001. [Online]. Available: https://www.iea.lth.se/publications/Theses/LTH-IEA-1027.pdf

[18] J. W. Judy, "Microelectromechanical systems (mems): fabrication, design and applications," *Smart Mater. and Struct.*, vol. 10, no. 6, p. 1115, nov 2001. [Online]. Available: https://dx.doi.org/10.1088/0964-1726/10/6/301

[19] P. Zwahlen *et al.*, "Navigation grade mems accelerometer," in *IEEE 23rd Int. Conf. on Microelectromech. Syst. (MEMS)*, 2010, pp. 631–634.

[20] M. Andrejašic, "Mems accelerometers," in *University of Ljubljana. Faculty for mathematics and physics, Department of physics, Seminar*, vol. 49, 2008.

[21] M. Li *et al.*, "Lorentz force magnetometer using a micromechanical oscillator," *Applied Physics Letters*, vol. 103, no. 17, p. 173504, 2013. [Online]. Available: https://doi.org/10.1063/1.4826278

[22] J. Valle *et al.*, "Design, fabrication, characterization and reliability study of cmos-mems lorentz-force magnetometers," *Microsystems & Nanoengineering*, vol. 8, no. 1, p. 103, 2022.

[23] K. Mohamadabadi, "Anisotropic magnetoresistance magnetometer for inertial navigation systems," Ph.D. dissertation, Ecole Polytechnique X, Paris, France, 2013. [Online]. Available: https://theses.hal.science/tel-00946970/

[24] M. Sfakiotakis, D. Lane, and J. Davies, "Review of fish swimming modes for aquatic locomotion," *IEEE J. of Ocean. Eng.*, vol. 24, no. 2, pp. 237–252, 1999.

[25] C. C. Lindsey, "Form, function, and locomotory habits in fish," *Fish physiol.*, vol. 7, pp. 1–88, 1978.

[26] O. Nordal, "Pike acceleration data," 2022, unpublished.

[27] R. W. Blake, "Fish functional design and swimming performance," *J. of fish biol.*, vol. 65, no. 5, pp. 1193–1222, 2004.

[28] P. Eklöv, "Group foraging versus solitary foraging efficiency in piscivorous predators: the perch, perca fluviatilis, and pike, esox lucius, patterns," *Animal Behaviour*, vol. 44, pp. 313–326, 1992.

[29] Thelma Biotel AS. Receivers. [Online]. Available: https://www.thelmabiotel.com/receiver/

[30] F. Broell, C. Burnell, and C. T. Taggart, "Measuring abnormal movements in free-swimming fish with accelerometers: implications for quantifying tag and parasite load," *J. of Exp. Biol.*, vol. 219, no. 5, pp. 695–705, 03 2016. [Online]. Available: https://doi.org/10.1242/jeb.133033

[31] Texas Instruments Inc., *MSP430FR247x Mixed-Signal Microcontrollers*, 3 2019 [Revised Sept. 2021], sLASE07C datasheet.

[32] Taiyo Yuden, *Wire-wound chip power inductors (CB series)*, 2021.

[33] Octave Forge. Demonstration 2. [Online]. Available: https://octave.sourceforge.io/signal/function/buttord.html

[34] ST microelectronics, *Ultra-compact high-performance eCompass module based on the LSM303AGR*, 4 2016, aN4825.

Appendix

A Acceleration Data exerpt

TagID	Timestamp	X	Y	Z	Temp. (°C)	Battery (V)
2_S1	05/03/2020 15:36:07.000	1.000	0.000	0.156	22.5	3.96
2_S1	05/03/2020 15:36:07.040	0.286	0.710	0.115		
2_S1	05/03/2020 15:36:07.080	2.101	1.333	0.010		
2_S1	05/03/2020 15:36:07.120	0.000	-0.584	0.070		
2_S1	05/03/2020 15:36:07.160	0.010	-0.790	0.074		
2_S1	05/03/2020 15:36:07.200	0.019	-0.900	0.031		
2_S1	05/03/2020 15:36:07.240	-0.045	-0.923	0.001		
2_S1	05/03/2020 15:36:07.280	-0.164	-0.942	-0.014		
2_S1	05/03/2020 15:36:07.320	-0.219	-1.009	0.020		
2_S1	05/03/2020 15:36:07.360	-0.196	-1.099	0.031		
2_S1	05/03/2020 15:36:07.400	-0.188	-1.100	-0.019		
2_S1	05/03/2020 15:36:07.440	-0.188	-1.039	-0.004		

B High-pass Filter Script

Modified script to make the butterworth filter used to remove g-vector from [33].

```
fs    = 50;
Npts  = fs / 2;
fstop = 0.02;
fpass = 0.1;
Rpass = 3;
Rstop = 20;
Wpass = 2 / fs * fpass;
Wstop = 2 / fs * fstop;
[n, Wn_p, Wn_s] = buttord (Wpass, Wstop, Rpass, Rstop);
[b, a] = butter (n, Wn_p, "high");
f = 8000:12000;
W = 2 * pi * f;
[H, f] = freqz (b, a, Npts, fs);
plot (f, 20 * log10 (abs (H)));
title ("Digital Butterworth high-pass : matching pass band");
xlabel ("Frequency (Hz)");
ylabel ("Attenuation (dB)");
grid on;
outline_hp_pass_x = [fpass(1), fpass(1), max(f)];
outline_hp_pass_y = [-80     , -Rpass  , -Rpass];
outline_hp_stop_x = [min(f)  , fstop(1), fstop(1), max(f)];
outline_hp_stop_y = [-Rstop  , -Rstop  , 0       , 0     ];
```

```
hold on;
plot (outline_hp_pass_x, outline_hp_pass_y, "m");
plot (outline_hp_stop_x, outline_hp_stop_y, "m");
ylim ([-80, 0]);
```

C Orientation Script

Script to find direction of acceleration peaks, by orienting relative to the g-vector. The g-vector is found by taking the first component of a fourier transform, which is 0Hz, or the same as the mean value.

```
fs    = 50;
Npts  = fs / 2;
fstop = 0.02;
fpass = 0.1;
Rpass = 3;
Rstop = 20;
Wpass = 2 / fs * fpass;
Wstop = 2 / fs * fstop;
[n, Wn_p, Wn_s] = buttord (Wpass, Wstop, Rpass, Rstop);
[b, a] = butter (n, Wn_p, "high");
f = 8000:12000;
W = 2 * pi * f;
[H, f] = freqz (b, a, Npts, fs);
plot (f, 20 * log10 (abs (H)));
title ("Digital Butterworth high-pass : matching pass band");
xlabel ("Frequency (Hz)");
ylabel ("Attenuation (dB)");
grid on;
outline_hp_pass_x = [fpass(1), fpass(1), max(f)];
outline_hp_pass_y = [-80     , -Rpass  , -Rpass];
outline_hp_stop_x = [min(f)  , fstop(1), fstop(1), max(f)];
outline_hp_stop_y = [-Rstop  , -Rstop  , 0       , 0     ];
hold on;
plot (outline_hp_pass_x, outline_hp_pass_y, "m");
plot (outline_hp_stop_x, outline_hp_stop_y, "m");
ylim ([-80, 0]);
```

NTNU
Norwegian University of
Science and Technology

THELMABIOTEL